Journal of the Air & Waste Management Association

ISSN: 1096-2247 (Print) 2162-2906 (Online) Journal homepage: https://www.tandfonline.com/loi/uawm20

Evaluation of Virtual Source Beam Configurations for Rapid Tomographic Reconstruction of Gas and Vapor Concentrations in Workplaces

Doo Y. Park , Michael G. Yost & Steven P. Levine

To cite this article: Doo Y. Park , Michael G. Yost & Steven P. Levine (1997) Evaluation of Virtual Source Beam Configurations for Rapid Tomographic Reconstruction of Gas and Vapor Concentrations in Workplaces, Journal of the Air & Waste Management Association, 47:5, 582-591, DOI: 10.1080/10473289.1997.10463687

To link to this article: https://doi.org/10.1080/10473289.1997.10463687

Published online: 01 Mar 2012.

TECHNICAL PAPER

ISSN 1047-3289 *J. Air & Waste Manage. Assoc.* **47**:582-591

Evaluation of Virtual Source Beam Configurations for Rapid Tomographic Reconstruction of Gas and Vapor Concentrations in Workplaces

Doo Y. Park
School of Public Health, University of Michigan, Ann Arbor, Michigan

Michael G. Yost
School of Public Health, University of Washington, Seattle, Washington

Steven P. Levine
School of Public Health, University of Michigan, Ann Arbor, Michigan

ABSTRACT

Beam path average data from an Open Path Fourier Transform Infrared (OP-FTIR) spectrometer can be used to reconstruct two-dimensional concentration maps of the gas and vapor contaminants in workplaces and the environment using computed tomographic (CT) techniques. However, a practical limitation arises because in the past, multiple-source and detector units were required to produce a sufficient number of intersecting beam paths in order to reconstruct concentration maps. Such a system can be applied to actual field monitoring situations only with great expense and difficulty. A single monostatic OP-FTIR system capable of rapid beam movement can eliminate this deficiency. Instead of many source and detector units, a virtual source arrangement has been proposed using a number of flat mirrors and retroreflectors to obtain intersecting folded beam paths.

Three virtual source beam configurations generated for a single-beam steerable FTIR system were tested using 54 flat mirrors and four retroreflectors or 54 flat mirrors and 56 retroreflectors mounted along the perimeter walls of a typical 24- x 21-ft test room. The virtual source CT configurations were numerically evaluated using concentration maps created from tracer gas concentration distributions measured experimentally in a test chamber. Synthetic beam path integral data were calculated from the test maps and beam configurations. Computer simulations of different beam configurations were used to determine the effects of beam geometry. The effects of noise and peak-reducing artifacts were evaluated. The performance of the tomographic reconstruction strategy was tested as a function of concentration and concentration gradients.

IMPLICATIONS

Computed tomographic techniques coupled with remote sensing have been applied to air monitoring. Three beam configurations were developed from an arrangement of flat mirrors and retroreflectors for use with a single-beam steerable OP-FTIR system. The beam configurations were numerically tested for various simulated and actual test maps. It has been concluded that these beam configurations used with a single OP-FTIR system could reproduce the general concentration gradient patterns and identify the concentration peak locations. This is the first proof-of-concept for a system applicable to real environmental monitoring situations.

INTRODUCTION

Open Path Fourier Transform Infrared (OP-FTIR) spectroscopy has found an increasing number of applications for indoor, environmental, and occupational air monitoring because it offers certain unique advantages.[1-3] Remote sensing allows for monitoring of inaccessible or isolated areas, eliminates pumps and tubing associated with conventional sample handling procedures, may offer improved recoveries of labile and polar compounds, and obviates the need for costly laboratory analysis. Consequently, sampling errors and sample losses are minimized once accurate reference spectra are obtained. OP-FTIR spectroscopy can also measure many compounds simultaneously in near real time.

One of the disadvantages of OP-FTIR techniques for use in environmental air monitoring is that the measurements furnish only path-integrated data; i.e., the measurement gives no information on spatial variation along the beam path. However, these path-integrated measurements

can be used directly to obtain spatially resolved data in a measurement plane with the technique of reconstructive tomography, also known as computed tomography (CT). The theory and concepts of computed tomography have been discussed,[4,5] and experimental trials relevant to occupational or indoor air monitoring applications recently were reported.[6]

Certain practical limitations arise in applying CT to indoor air or environmental monitoring. CT requires input data consisting of multiple views of intersecting beam paths to produce the data necessary to reconstruct concentration maps. A fan beam configuration was proposed in conjunction with optical tomography for mapping iodine vapor density in a plane, but it also requires numerous detectors.[7] Most of the theoretical studies to date are contingent upon using a large number of source and detector units, which are prohibitively expensive and unrealistic in most conceivable field situations.[4,5] For example, an MCT detector typically used for these applications costs about $10,000.

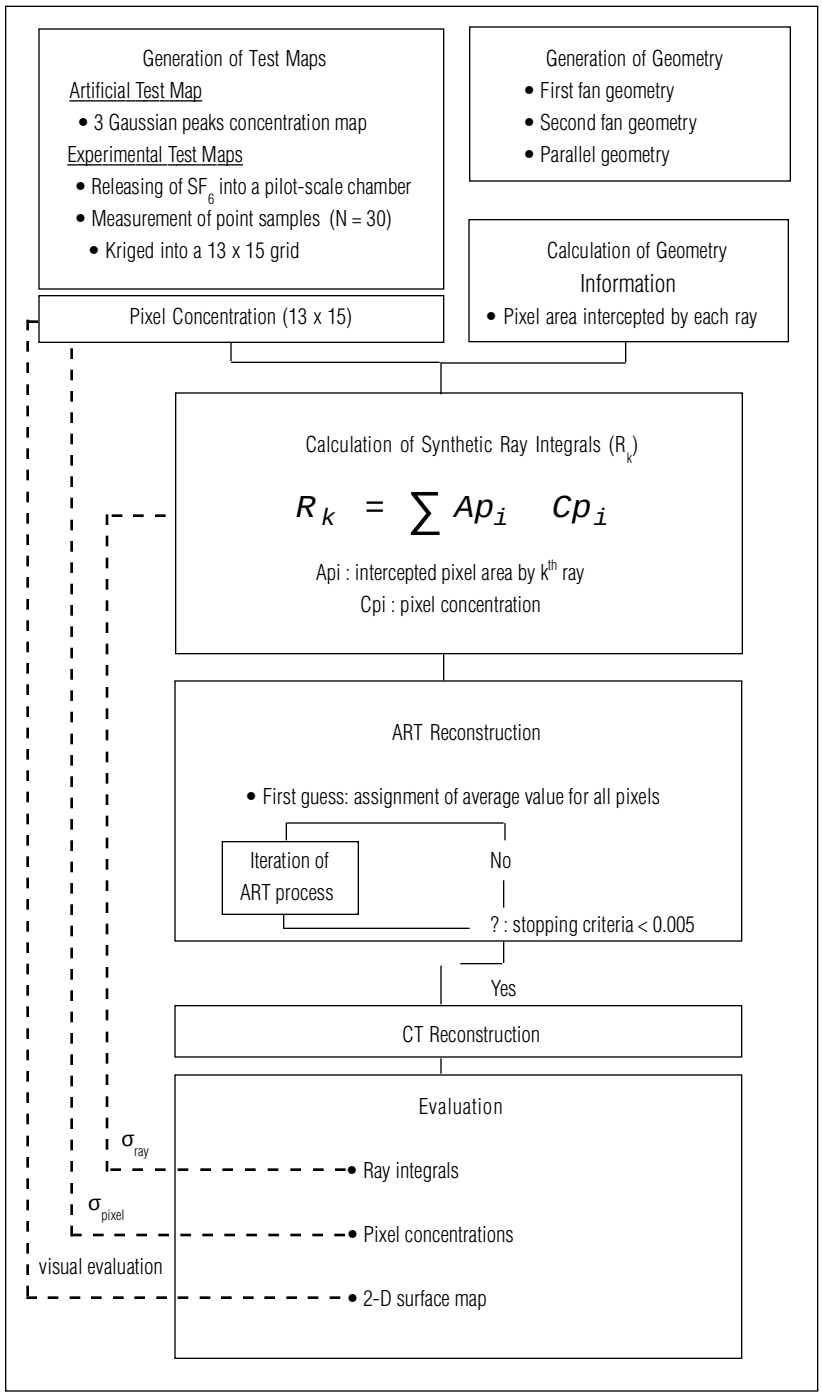

Figure 1. Summary of the stimulation test procedure for evaluation of beam configurations.

This limitation was overcome by using a commercially available beam-steerable OP-FTIR system capable of fast beam movement, which has been developed. This OP-FTIR configuration uses a beam splitter that allows the IR source, interferometer, and detector to be housed in a single module, equipped with a single telescope for sending and receiving the IR beam. A steerable flat mirror is installed in this monostatic OP-FTIR system to rapidly move the IR beam. A mirror or retroreflector is used to reflect the IR beam at the end of each path. Therefore, multiple beam paths can be generated by using a number of flat mirrors or retroreflectors. Several simulation tests have been reported to explore CT reconstructions of air pollutants with this instrument. In the previous studies, at least two systems were used for the simulated tests, and four systems were recommended for obtaining reliable results. These simulations were conducted with the use of synthetic test maps having narrow, symmetrical, distinct Gaussian peaks on a zero-level background, which are never present in actual situations and are relatively easy to reconstruct.[8]

We propose a method for obtaining data for CT reconstructions from an arrangement of many flat mirrors and retroreflectors with the use of a single, fast-beam steerable system, instead of multiple-source and detector units. This method can be cost effective and practical because of the use of a single OP-FTIR system. Three beam configurations were created based on various combinations of flat mirrors, retroreflectors, and a commercial OP-FTIR. Both a synthetic Gaussian peak gradient and various actual concentration gradients, obtained from pilot-scale chamber experiments, were tested for realistic applications of CT techniques.

In general, numerical evaluation of the performance of an FTIR/CT system prior to actual application is desirable because an actual test requires high cost and intensive

labor. Thus, a computer simulation program was used to evaluate three beam configurations proposed in this study. This paper reports the simulation reconstruction results from these beam configurations.

METHODS

The simulation test procedure is summarized in Figure 1. Four concentration gradient maps were generated from pilot-scale chamber experiments to test realistic applications, and one synthetic test map having three narrow Gaussian peaks was created to compare with the test maps from experiments, as shown in Figures 5(a) and 9(a). A total of 195 pixel values were obtained by Kriging into a 13 x 15 grid map. Three-beam configurations were created, based on the size and number of flat mirrors and retroreflectors (Figures 2-4). Pixel areas intercepted by the rays for each geometry were calculated. Fifty-six beam path integrals for the first fan geometry, 100 for the second fan geometry, and 112 for the parallel geometry were obtained by summation of productions of pixel concentration and pixel area intercepted by the beam paths. The beam path integral data were used for the CT reconstruction process. CT reconstructions were evaluated by comparison with the test maps.

Test Concentration Gradients

One synthetic concentration map was generated as shown in Figure 5(a). This synthetic concentration map has three Gaussian peaks on a zero-level background. The peaks have different locations and heights. This map was chosen, despite the fact that Gaussian peaks on zero background are never found in actual practice, in order to facilitate the comparison of our results with those obtained by other investigators.[4,5,8,13]

Concentration gradients to test CT reconstructions of air pollutant concentrations should be representative of real situations. In this study, concentration measurements were collected in an experimental chamber to provide representative concentration profiles for the evaluation of beam configurations. The dimensions of the chamber were 24 x 21 x 8 ft. The chamber has controlled ventilation producing approximately uniform horizontal flow. Sulfur hexafluoride (SF_6) tracer gas was released at a constant emission rate from 1-inch spherical ceramic point-source diffusers into the stationary flow field of the chamber.

Air samples were obtained at 30 points averaged over one hour during stable concentration gradient conditions. SF_6 concentrations were analyzed using a Bruel and Kjaer

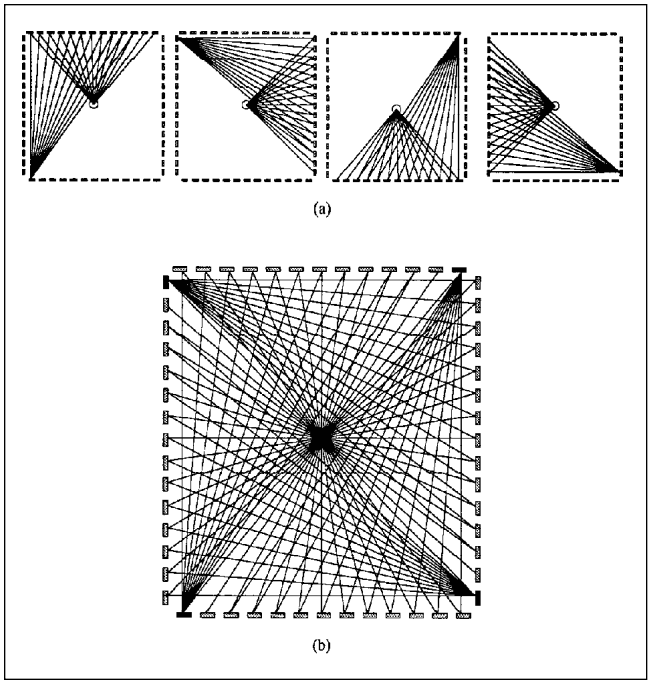

Figure 2. Schematic representation of the first fan geometry with 52 flat mirrors and four retroflectors at the perimeter of the room. A fast beam movement OP-FTIR system is placed at the center. (a) Each view of four projection angles. Fifty-two flat mirrors were placed along the perimeter of the chamber and a retroflector at each of the four corners. (b) Total beam configuration. Gray rectangles represent flat mirrors and black ones represent retroflectors. Solid lines represent beam paths.

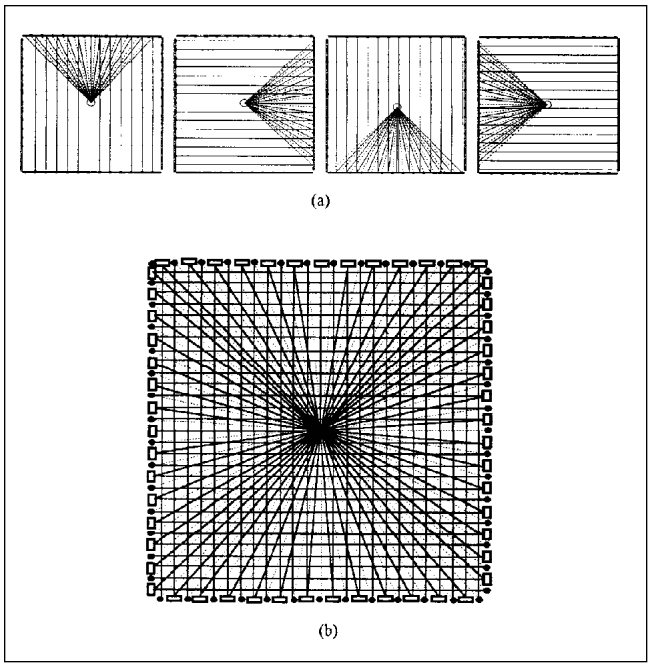

Figure 3. A schematic representation of the second fan geometry with 52 flat mirrors and 44 small and eight large retroflectors placed at the perimeter of the room. A fast beam movement OP-FTIR system is placed at the center. (a) Each view of the projection angles. Fifty-two flat mirrors were placed along the perimeter of the chamber and two retroflectors at each of the four corners. Additional 44 small retroflectors were placed between the flat mirrors. (b) Total beam configuration. Black rectangles represent small retroflectors and white rectangles represent flat mirrors. Black circles represent short beam paths from OP-FTIR to small retroflectors.

1302 photo-acoustic detector (Bruel and Kjaer Instruments, Marlborough, MA). The SF_6 data measured at the 30 sample locations were Kriged into a 13 x 15 grid using the computer program SURFER (Golden Software, Golden, CO) to generate two-dimensional least-squares fitted concentration maps. Various concentration patterns were obtained by changing the number, locations, and emission rates of the SF_6 sources. For this study, four different concentration maps were selected for testing as shown in Figures 6(a), 7(a), 8(a), and 9(a).

Beam Configurations

This study was designed for a pilot-scale chamber that was used to obtain the test concentration gradients. The pixel size was set at 1.6 x 1.6 ft resulting in a 13 x 15 CT reconstruction grid.

This design uses flat mirrors to generate the intersected beam paths by redirecting the beam originating from the beam steerable OP-FTIR to a reflector located on an opposing wall. It was necessary to use retroreflectors (corner cube arrays) to return the infrared beam to the OP-FTIR system because, in practice, it is extremely difficult to align the beam using two flat mirrors. In addition, retroreflectors allow multiple beams to return from multiple flat mirrors to each of them. Thus, a single retroreflector could reflect the beams from many different flat mirrors to the same point within an acceptance angle of 22°.

Three beam configurations were selected for testing in this study: (1) a first fan geometry with a beam-steerable OP-FTIR at the center of the chamber, 52 flat mirrors placed along the perimeter of the chamber, and a retroreflector at each of the four corners; (2) a second fan geometry with a beam-steerable OP-FTIR at the center of the chamber, 52 flat mirrors placed along the perimeter of the chamber, two retroreflectors at each of the four corners, and 44 small retroreflectors placed in-between the flat mirrors; and (3) a parallel geometry with a beam-steerable OP-FTIR system placed at center of the chamber, 56 flat mirrors placed along the perimeter of the chamber, and 56 small retroreflectors placed between the flat mirrors.

The first fan geometry (Figure 2) created a network of 56 intersecting beam paths that were used as data input for the CT program. The second fan geometry (Figure 3) created a network of 100 beam paths: 48 intersecting beam paths with eight projection angles and 52 radial beam paths to the retroreflectors. The parallel geometry (Figure 4) created a network of 112 beam paths. The parallel geometry had 56 folded beam paths that traveled to retroreflectors (shown as circles) via flat mirrors (shown as rectangles). Interleaved with the folded beam paths are 56 short radial beam paths directly from the OP-FTIR to the retroreflectors.

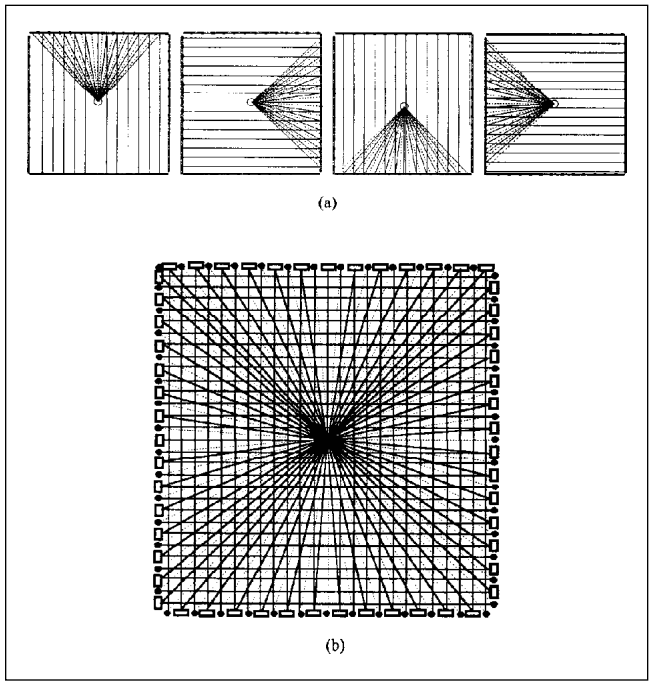

Figure 4. Schematic representation of the parallel geometry with 54 flat mirrors and 56 retroflectors at the perimeter of the room. A fast beam movement OP-FTIR system is placed at the center. (a) Each view of four projection angles. Fifty-six flat mirrors were placed along the perimeter of the chamber and 56 small retroflectors were placed between the flat mirrors. (b) Total beam configuration. Rectangles represent retroflectors and black coircles represent small retroflectors. Solid lines represent folded beam paths, and dot lines represent short beam paths from OP-FTIR to small retroflectors.

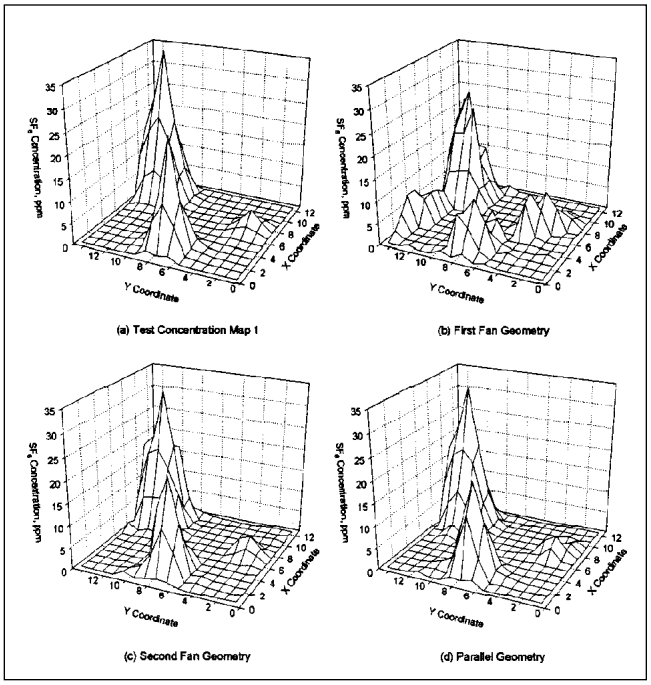

Figure 5. Reconstruction maps with each beam configuration for SF_6 concentration profile of single peak. (a) Test concentration map, (b) first fan geometry, (c) second fan geometry, and (d) parallel geometry.

The limited acceptance angle of the retroreflectors created additional constraints on the fan geometry. Figure 2 shows a schematic of the beam configuration of the first fan geometry using 52 flat mirrors and four large retroreflectors typical for this OP-FTIR system, with one retroreflector placed at each corner. The 12- x 12-inch retroreflector was used to efficiently reflect an 8 inch IR beam. Twelve flat mirrors are shown along each short side wall (the horizontal side in the figure). Eleven of these mirrors could be used to generate folded rays to a retroreflector, but beam paths via the remaining flat mirrors would not be reflected from retroreflectors. This conclusion was based on previous tests which indicated a 22° acceptance angle for retroreflectors used in this test. Instead, these beam paths were directed straight back to the FTIR. Similarly, 14 flat mirrors were placed along each long side, but only 13 folded beam paths were generated.

Figure 3 shows a schematic of the beam configuration for the second fan geometry, using 48 flat mirrors as well as eight large and 44 small retroreflectors placed along the perimeter of the wall. Eleven flat mirrors are shown along each short side wall (the horizontal side in the figure). Six of these mirrors were oriented to one of the large retroreflectors at the opposite corner, and five of them were oriented to the other large retroreflector. Similarly, 14 flat mirrors were placed along each long side, and seven and six of them were oriented to the large retroreflectors at the opposite corners.

The IR beam width of the horizontal plane for the first fan geometry was 8 inches, corresponding to the beam width in the commercial fast-beam steerable FTIR system. However, for the second fan and parallel geometries, the effective beam width was limited to 4 inches due to the size of retroreflectors used. Low-cost, small retroreflectors were employed since the cost factor was significant for installation of a large number of them. Although a telescope collimates the IR beam, a commercial OP-FTIR has a slight beam divergence of 3.3 milliradians. However, it was small enough to be neglected in this study because beam paths were relatively short.

Simulation Tests

A program written in Turbo PASCAL (Borland, Scotts Valley, CA) was used to calculate a geometry file which provided information on the intersection (length) of each beam path with each pixel. From these geometry files, path integral data for the fan and parallel geometries were obtained from each Kriged input map by calculating the sum of concentrations of the pixel times pixel area intercepted by the beam path. The calculated path integral data for the beam configurations were used to generate CT reconstructions of the two-dimensional concentration maps.

A program written in Turbo PASCAL was used to implement the algebraic reconstruction technique (ART)

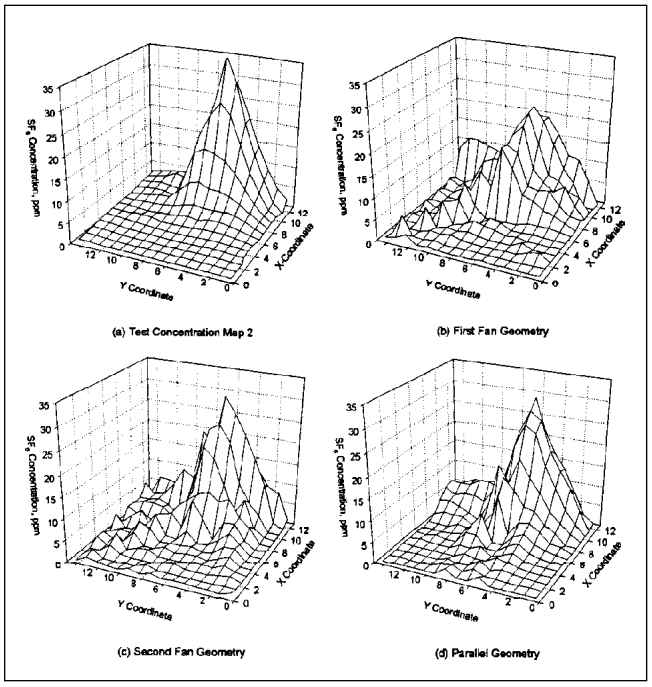

Figure 6. Reconstruction maps with each beam configuration for SF_6 concentration profile of single peak. (a) Test concentration map, (b) first fan geometry, (c) second fan geometry, and (d) parallel geometry.

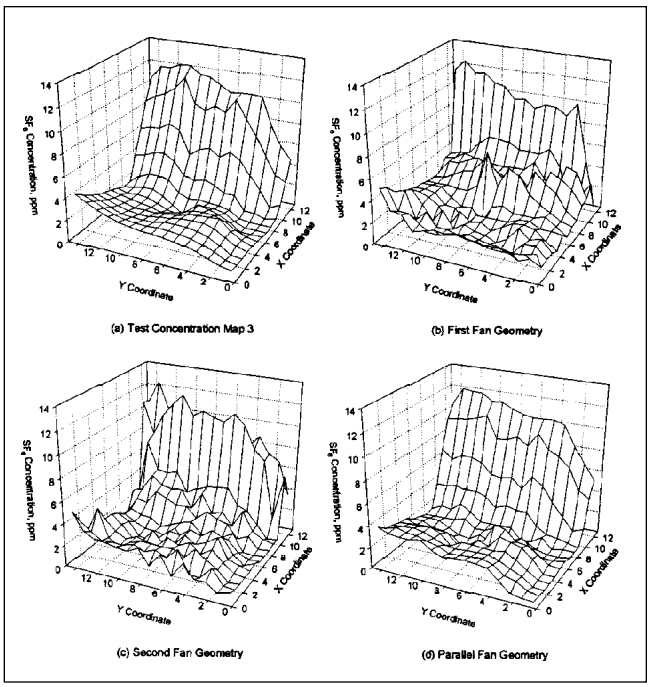

Figure 7. Reconstruction maps with each beam configuration for slanted SF_6 concentration profile. (a) Test concentration map, (b) first fan geometry, (c) second fan geometry, and (d) parallel geometry.

algorithm for the CT reconstructions. The ART algorithm is described elsewhere in the literature.[9] This algorithm iteratively adjusts the concentration in each pixel area intersected by a beam path to maximize the agreement between the input (or true) beam path measurement and the same path in the CT reconstructed map. The initial concentration value for each pixel was set at the average concentration for all rays. The only constraint applied to the reconstruction procedure was that the pixel concentration should not be negative. Thus, after each iteration, negative pixel values were assigned as a value of zero at each iteration.

After each iteration, a value of σ_{ray} was calculated as a convergence criterion indicating the overall agreement between the true ray integrals and the calculated ray integrals from reconstructed concentration map after a given iteration:[6,10,11]

$$\sigma_{ray} = \sqrt{\frac{\sum_{k=1}^{n}\left(R_{true,i} - R_{recon,i}\right)^2}{\sum_{k=1}^{n} R_{true,i}^{\ 2}}} \qquad (1)$$

where $R_{true,i}$ is the experimental or synthetic ray integral value of the i^{th} ray. $R_{recon,i}$ is the calculated ray integral value of the k^{th} ray from the CT reconstruction. A lower value of σ_{ray} indicates a better agreement between the average concentrations along the rays of the reconstruction and the true data (calculated from the original test map). For perfect agreement, σ_{ray} is zero.

However, a small value of σ_{ray} does not necessarily reflect agreement of each pixel concentration between the true map and the reconstruction. The σ_{ray} values indicate only relative convergence for a given concentration profile. Thus, this value cannot be used to compare the convergence among different concentration profiles.

The σ_{ray} value was also used as a stopping criteria for the iteration process. The reconstruction was terminated when the fractional change in σ_{ray} from one iteration to the next was less than 0.005. The fraction change was defined as follows:

$$\text{Fraction change} = \frac{\sigma_{ray,\,k+1} - \sigma_{ray,\,k}}{\sigma_{ray,\,k}}$$

where $\sigma_{ray,\,k}$ and $\sigma_{ray,\,k+1}$ is the σ_{ray} values of the k^{th} and $(k+1)^{th}$ iterations respectively. There is no universal quantitative method to evaluate reconstruction quality. Several quantitative terms have been developed and used for evaluation of two images.[4,6,11] However, they all are not absolute numbers and they can be used only for comparison of images having the same concentration gradient profile.

A perimeter σ_{pixel} is defined to quantify the overall

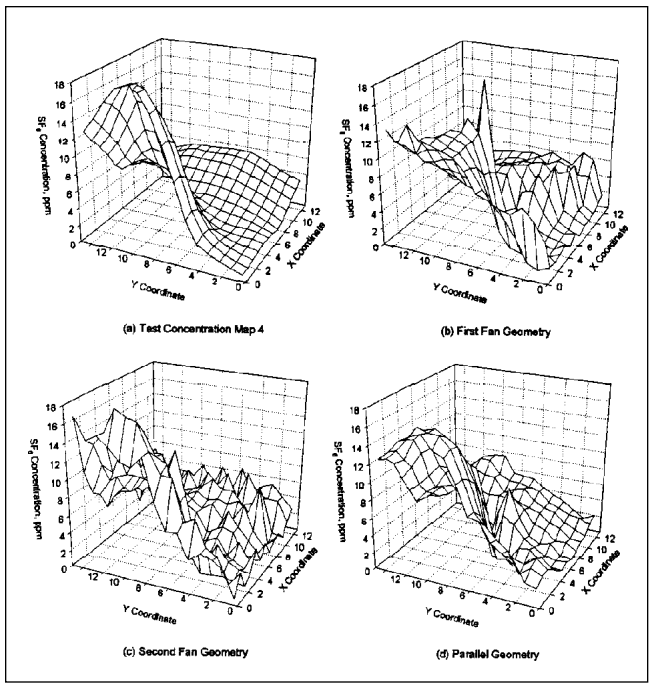

Figure 8. Reconstruction maps with each beam configuration for SF_6 concentration profile of two broad peaks. (a) Test concentration map, (b) first fan geometry, (c) second fan geometry, and (d) parallel geometry.

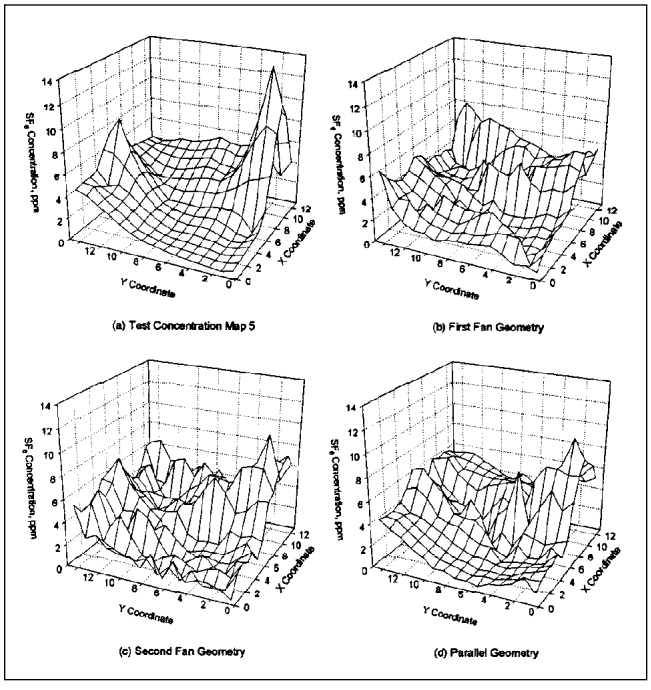

Figure 9. Reconstruction maps with each beam configuration for SF_6 concentration profile of the two peaks. (a) Test concentration map, (b) first fan geometry, (c) second fan geometry, and (d) parallel geometry.

agreement of the pixel concentrations between the CT reconstruction and the true map. This parameter has been used to evaluate the quality of the reconstructions in this and other studies.[6,11] It is calculated as:

$$\sigma_{pixel} = \sqrt{\frac{\sum_{p=1}^{n} \left(C_{p,\,test} - C_{p,\,recon} \right)^2}{\sum_{p=1}^{n} C_{p,\,test}^{\,2}}}$$

where $C_{p,\,test}$ is the concentration in a pixel obtained from the test (true) map and $C_{p,\,recon}$ is the pixel concentration calculated from the reconstruction map. The value of σ_{pixel} reflects the degree of matching between the pixel's concentrations in the test map and the reconstruction map. A value of zero for σ_{pixel} indicates a perfect reconstruction; a lower value indicates better agreement between the CT reconstruction and the true map. Again, it is a relative parameter rather than an absolute value for a given concentration gradient. Thus, this can be used to compare the degree of agreement of the CT reconstruction to the true map only for a given test map (i.e., a value of the s_{pixel} has no meaning for comparisons among different test maps).

We selected the ART algorithm because it works well with a limited number of projection angles, or where the projections are not uniformly distributed over 180° or 360°.[12] Thus it can easily accomodate the various folded beam geometries and it produces reconstructions with relatively sparse input data.

Table 1. Summary of the parameters of the reconstructions.

Test Map	First Fan		Second Fan		Parallel	
	σ_{ray} *	σ_{pixel} **	σ_{ray} *	σ_{pixel} **	σ_{ray} *	σ_{pixel} **
Map 1	0.15	45.4	0.26	16.7	0.23	11.4
Map 2	< 0.1	42.0	< 0.1	26.7	2.59	24.6
Map 3	18.6	43.8	1.15	23.6	0.36	10.6
Map 4	< 0.1	32.5	0.80	24.8	0.40	19.6
Map 5	< 0.1	39.4	1.16	30.1	0.88	26.3

*σ_{ray} (x 10^2): A lower value of σ_{ray} indicates a better agreement between the average concentrations along the rays of the reconstruction and the true data (calculated from the original test map). For perfect agreement, σ_{ray} is zero.

** σ_{pixel} (x 10^3): The value of σ_{pixel} reflects the degree of matching between the pixel concentrations in the test map and the reconstruction map. A value of zero for σ_{pixel} indicates a perfect reconstruction; a lower value indicates better agreement between the CT reconstruction and the true map.

RESULTS AND DISCUSSION

Test Concentration Gradient Maps

Concentration gradients to test CT reconstructions of air pollutant concentrations should be representative of real situations. Bivariate normal distributions have frequently been used to generate synthetic concentration gradients of chemicals in previous studies. However, these synthetic test maps, having narrow, distinct Gaussian peas, may be unsuitable to test actual environmental monitoring applications of CT techniques.[4,5,8,13]

Although Gaussian peaks are convenient, there is little evidence that the concentration gradients of gas and vapor pollutants in actual workplaces or the environment would be Gaussian peaks. Turbulent air motion generated by movement of workers and machines, external air movement, temperature gradients, etc., would continuously mix pollutants. Concentration gradient maps obtained from chamber experiments showed different patterns (Figures 6(a), 7(a), 8(a), and 9(a)) from the artificial synthetic Gaussian peak profile (Figure 5(a)). Thus, the concentration gradients obtained from these chamber experiments were judged more suitable than those modeled by bivariate normal distributions.

A second disadvantage of test maps based on narrow, distinct Gaussian peaks is that a relatively small fraction of the beam paths intersect the peaks. These beam measurements can be redistributed easily into the original peak locations. The rest of the beam paths having zero-level measurements constrain the concentration of background level pixels. This is clearly shown by comparing the reconstruction results, as shown in Figures 5 and 9. Good reconstructions were achieved for Test Concentration Map 1, which has three narrow, distinct Gaussian peaks with both second fan and parallel geometries, as shown Figure 5. On the other hand, reconstruction maps showed poor quality for Test Construction Map 5, which has two peaks on a realistic background concentration gradient, as shown in Figure 9. It was clearly seen from the visual reconstruction maps that the reconstruction simulation tests for the different concentration gradients resulted in different conclusions.

This result implies that experimentally based concentration maps should be used as the primary test of CT reconstruction for environmental monitoring. The number of narrow, distinct Gaussian peaks does not generally reflect the complexity or difficulty of the test map for evaluating CT reconstructions. Therefore, one should be careful in interpreting simulation results obtained using only synthetic concentration maps having narrow Gaussian peaks, since this could result in misleading conclusions.

First Fan Geometry

Five different concentration maps were used to evaluate the three beam geometries. Ideally the CT reconstructions should exactly match the test maps since these reconstructions come from noise-free input data. Any differences are due to artifacts introduced by the reconstruction process.

All reconstructions with the first fan geometry show smeared and broadened peaks (Figures 5(b), 6(b), 7(b), 8(b), and 9(b)). All peak heights were reduced and artificial peaks appeared that were relatively higher than those obtained when performing reconstructions with the second fan and parallel geometries. These artifacts clearly resulted from a decreased number of rays and projection angles. In addition, the concentration of beam paths in the area near the corner retroreflectors and OP-FTIR could result in insufficient spacial information to accurately reconstruct the original test maps.

However, the first fan geometry may be useful in many real situations, since good qualitative reconstructions were achieved in terms of peak locations and concentration gradient patterns. Ideally, CT reconstruction should perfectly match the original maps with a sufficient number of rays and projection angles. There are certain practical limitations, such as limited resources, to getting sufficient data for CT reconstructions in actual practice. Still, this fan geometry could be applied in many field situations for leak location detection and alarm monitoring when high accuracy determination of actual concentrations may not be crucial.

Another advantage of the first fan geometry would be the relatively short time for a complete sweep of the entire measurement plane. However, concentration gradient patterns would continuously change during collection of the beam path measurements, resulting in inconsistency among the beam measurements in a real situation. Therefore, in practice, it is very important to reduce the measurement time for a complete sweep of the entire measurement plane. It is clearly possible to reduce the measurement time with fewer beams.

However, because of poor reconstructions for complex concentration gradients, this geometry should be applied only in limited situations such as relatively simple concentration gradient areas.

Second Fan Geometry

The second fan geometry produced greatly improved reconstructions compared with the first fan geometry. By visually comparing the CT maps to the original concentration maps and to each other, the position of the concentration peak at the source was correctly located and steep concentration gradients around the source were reproduced. However, many pixel concentrations showed high and steep gradients. These unrealistic artifacts were observed in most reconstructions.

Figure 5(c) shows the reconstruction for Test Map 1. Peaks were slightly broadened and peak heights were slightly reduced. However, a fairly good reconstruction was obtained. Peak locations exactly matched originals and peak height was not smeared into low concentration areas. No artifacts were observed in low concentration areas.

The CT maps calculated from the experimentally Kriged data for comparison are shown in Figures 6(c), 7(c), 8(c), and 9(c). In comparing these CT maps to the original Kriged concentration maps, the concentration maxima were located correctly, along with adjacent steep concentration gradients. The same trends noted above for the first test map emerged, but the quality of reconstructions was greatly improved. For Test Maps 4 and 5, peak heights were reduced and smearing of high concentration areas into low concentration areas was observed.

The quality of reconstruction maps with the second fan geometry was significantly improved in terms of the σ_{pixel} (Table 1), in addition to the improvement noted using qualitative visual assessment. The σ_{pixel} values of the first fan geometry for all tests maps were significantly higher than those of the second fan geometry. On the other hand, the σ_{ray} values for the first fan geometry, except Test Map 3, were much lower than those of the second fan and parallel geometries. Very low σ_{ray} values mean that the ART algorithm generated reconstructions with valid solutions. However, this does not imply that reconstructions match the test maps. It is clearly seen from Figure 6 that ART did not converge to the true solution with very low σ_{ray} values. Therefore, the σ_{ray} values may not be a useful indicator to predict the quality of reconstructions.

The σ_{pixel} values of the second fan geometry were slightly larger than those of the parallel geometry, although the concentration gradient patterns were similar between maps of the second fan and parallel geometries. This can be explained by the unrealistic artifacts shown in reconstructions of the second fan geometry.

As discussed, values of the σ_{ray} do not necessarily correlate with the actual reconstruction quality. It is apparent from Table 1 that the ART algorithm found an almost perfect solution to distribute the ray integrals to the pixels for the first fan geometry. This is demonstrated by the low values of σ_{ray} (except for the Test Map 3). However, the values of σ_{pixel} for the first fan geometry were relatively higher than the second fan and parallel geometries; i.e., the pixel concentrations were reproduced incorrectly. This could lead to the false conclusion that

a reconstruction would be better with a lower value of the σ_{ray} because σ_{ray} is the only parameter available for ART processing of experimental ray data. In an actual situation, it may be the only parameter available to assess the quality of the reconstruction map without measuring the distribution of the air contaminant with a second method. Therefore, CT reconstruction strategies must be evaluated with known test maps having a variety of concentration gradient patterns before field applications.

Parallel Geometry

The parallel geometry produced the best overall agreement between test maps and reconstructions. Based on the value of σ_{pixel} for each map in Table 1, the parallel geometry also appeared to reproduce the input map with the best fidelity in every case. This trend is also visually shown in Figures 5, 6, 7, 8, and 9, although some residual artifacts still appeared in low concentration areas. It is concluded that the parallel geometry is generally superior than the fan geometries when using a monostatic OP-FTIR system.

Two factors can be considered as main contributors to the improved reconstructions obtained with the parallel geometry: (1) the even distribution of beam paths and (2) an increase in the number of beam paths. Evenly distributed beam paths are more efficient for calculating each pixel concentration during the reconstruction process. Reconstruction quality will also be improved by using more beam paths. The parallel geometry has 112 beam paths, which is 12% greater than that of the second fan geometry.

Although peak-smearing effects and minor artifacts were still observed, the fact that the general concentration gradient patterns were successfully reproduced and the peak locations were recognized is significant. Because the geometry is not the sole factor that affects the quality of reconstructions, there may be more room to improve zero-pixel constraints in the solution space. Although the ART algorithm can distribute the ray integrals to pixels and achieve a good match between the true ray integrals and the calculated ray integrals from the reconstructed map, the solutions are unrealistic at a pixel level.

This is due to the underdetermined condition that unknown pixel values (195) are superior than known ray data. The ratio of the number of pixels to the number of rays was 3.48 for the first fan geometry, 1.95 for the second fan geometry, and 1.74 for the parallel geometry. Todd et al. have proposed in previous simulation work that good reconstructions could be achieved in highly underdetermined (ill-conditioned) conditions with a ratio of pixels to rays up to 6.7.[4,13] However, those studies evaluated favorable conditions using multiple optical sensing systems and unrealistic, less challenging synthetic Gaussian concentration profiles (similar to Test Map 1 in this study). In contrast, geometries in this present study have fewer projection angles and the rays were distributed unevenly. Furthermore, test maps which were experimentally taken were more complex in this study.

CONCLUSIONS

Three beam configurations suitable for the application of computed tomographic reconstructions to OP-FTIR measurements in workplace and environmental applications were tested. These beam configurations used an array of many flat mirrors and retroreflectors to produce intersecting beam paths. Input test maps were created from both a synthetic bivariate normal distribution model and air sample data obtained from experimentally measured tracer gas concentrations generated in a test chamber.

It was necessary to evaluate all realistic concentration gradients for each CT method because reconstruction results vary with different concentration gradient profiles. Test maps which have several peaks and broad concentration gradients over many pixels were the most complex and difficult to reproduce from the original image because of increased indeterminacy. On the other hand, relatively good reconstructions were easily achieved for a synthetic test map having three narrow Gaussian peaks on a zero-level background. Therefore, a distinct, narrow Gaussian peak concentration profile may produce an unsuitable test of CT reconstruction methods for air monitoring.

Generally, peak heights were reduced and reconstructed peaks appeared smeared or broadened over many lower concentration pixels, particularly in the first fan geometry. The first fan geometry consisted of 56 rays and required less resources. Thus, it provides short measurement time and relatively low cost. However, it can be applied only in limited situations because poor reconstructions were reproduced, especially for complex concentration profiles. The second fan geometry could greatly improve the reconstructions compared to the first fan geometry. However, it was not superior to the parallel geometry. The best agreement was found between the reconstructed maps and the original test maps using the parallel geometry with 54 flat mirrors and 56 retroreflectors. In each case, reconstructed maps for the parallel geometry contained minor artifacts at lower concentration areas. These artifacts increased for complicated concentration gradients.

All reconstructed maps show some unrealistic artifacts, in the form of very steep and high concentration gradients at some pixels. This was due to the characteristics of the ART algorithm, which calculates pixel concentrations without considering adjacent pixel concentrations. Therefore, further study is needed for the development of new algorithms which can link the pixel concentrations during the reconstruction process.

Although minor artifacts and unrealistically steep and high concentration gradients were still observed, the parallel geometry could directly be applied in many industrial situations with reasonable cost and resources.

ACKNOWLEDGMENTS

The authors would like to thank Zhou Yi, Jyunde Wu, and Robert Spear at the University of California at Berkeley for assistance with the experiment. The authors also thank MDA Scientific, Inc., (now Environmental Technologies Group, Inc. (ETG)) for technical support. This study was supported by NIOSH grant 1R01-OH02666.

REFERENCES

1. Xiao, H.K.; Levine, S.P.; Herget, W.F.; D'Arcy, J.B.; Spear, R.; Pritchett, T. "A transportable remote sensing infrared air monitoring system," *Am. Ind. Hyg. Assoc. J.* **1991**, *52*, 449.
2. Levine, S.P.; Russwurm, G.M. "FTIR optical remote sensing for monitoring airborne gas and vapor contaminants," *Trends in Anal. Chem.* **1994**, *13*(7), 258.
3. Malachowski, M.S.; Levine, S.P.; Herrin, G.; Spear, R.C.; Yost, M.G.; Zhou, Y. "Workplace and environmental air contaminant concentrations measured by OP-FTIR spectroscopy: a statistical process control technique to detect changes from normal operating conditions," *J. Air & Waste Manage. Assoc.* **1994**, *44*, 673.
4. Todd, L.; Leith, D. "Remote sensing and computed tomography in industrial hygiene," *Am. Ind. Hyg. Assoc.* J. **1990**, 51(4), 224.
5. Todd, L.; Ramachandran, G. "Evaluation of algorithms for tomographic reconstruction of chemical concentrations in indoor air," *Am. Ind. Hyg. Assoc. J.* **1994**, *55*(5), 403.
6. Yost, M.G.; Gadgil, A.J.; Drescher, A.C.; Zhou, Y.; Sigmond, M.A.; Levine, S.P.; Nazaroff, W.W.; Saisan, P.A. "Imaging indoor tracer-gas concentrations with computed tomography: experimental results with a remote sensing FTIR system," *Am. Ind. Hyg. Assoc. J.* **1994**, *55(5),* 395.
7. Bennett, K.E.; Faries, G.W.; Byer, R.L. "Experimental optical fan beam tomography," *Appl. Opt.* **1984**, *23(*18*),* 2678.
8. Todd, L.; Ramachandran, G. "Evaluation of optical source-detector configurations for tomographic reconstruction of chemical concentrations in indoor air," *Am. Ind. Hyg. Assoc. J.* **1994,** *55(*12*),* 1133.
9. Brooks, R.A.; Di Chiro, G. "The theory of image reconstruction in computed tomography," *Radiology* **1975**, *117*, 561.
10. Drescher, A.C.; Park, D.Y.; Yost, M.G.; Gadgil, A.J.; Levine, S.P.; Nazaroff, W.W. "Chamber studies of trace gas concentration measurements using open path FTIR remote sensing and SBFM computed tomography," submitted to *Atmospheric Environment* 1995.
11. Drescher, A.C.; Gadgil, A.J.; Nazaroff, W.W. "Novel approach for tomographic reconstruction of gas concentration distributions in air: use of smooth basis functions and simulated annealing," submitted to *Atmospheric Environment* 1994.
12. Kak, A.C.; Slaney, M. *Principles of Computerized Tomographic Imaging*; IEEE Press: New York, 1988.
13. Ramachandran, G.; Leith, D.; Todd, L. "Extraction of spatial aerosol distributions from multispectral light extinction measurements using computed tomography," *J. Opt. Soc.* **1993,** *11*.

About the Authors

Doo Y. Park, corresponding author, is an assistant professor of environmental safety engineering at Hansung University. Recently, he received the Dr.P.H. from the University of Michigan. Winner of the 1995 Warren A. Cook Award, he has worked at Korean NIOSH after receiving his MPH from Seoul National University. His address is: Department of Environmental Safety Engineering, Hansung University, 389 Samsun-dong 2 Ga, Sung Guk-ku, Seoul 136-792 Korea; e-mail: dyp1@chollian.net. Michael G. Yost is assistant professor of environmental health, School of Public Health, University of Washington, and co-principal investigator of NIOSH Grant R01-OH02666. His address is: Department of Environmental Health, University of Michigan, Seattle, WA 98195; e-mail: airion@u.washington.edu. Steven P. Levine is professor of occupational and environmental health, and director of NIOSH Grant R01-OH02666. He was the thesis advisor of Doo Y. Park. He can be reached at: Department of Environmental and Industrial Health, School of Public Health, University of Michigan, Ann Arbor, MI 48109-2029; e-mail: SLIH@umich.edu.